J Mater Sci (2009) 44:5842–5851
DOI 10.1007/s10853-009-3824-x

A novel approach to the prediction of long-term creep fracture: with application to 18Cr–12Ni–Mo steel (plate and bar)

M. Evans

Received: 20 April 2009 / Accepted: 18 August 2009 / Published online: 29 August 2009

Abstract Designers of new power-generation plants are looking to make use of new and existing high-strength austenitic steels so that these plants can operate with much higher steam and therefore metal temperatures. However, this article shows that the recently developed Wilshire–Scharning methodology is incapable of producing accurate long-term life predictions of these materials from short-term data. This article puts forward a modification of this approach that should enable existing and newly developed austenitic stainless steels to be brought into safe operation more cost effectively and over a quicker time span. Estimation of this model showed that the activation energy for creep was dependent on whether the test stress was above or below the yield stress. Analysis of the results from tests lasting only up to 5,000 h accurately predict the creep lives for stress–temperature conditions causing failure in 100,000 h or more.

Introduction

Today's power stations predominantly use ferritic or martensitic resistant steels for steam generation and operate at temperatures of not more than 873 K, with the use of austenitic steels being confined to boiler tubing. In order to raise the efficiency of future power generation, new plants will have to operate with much higher steam and therefore metal temperatures. However, the low alloy steels such as 0.5Cr–0.5Mo–0.25 V, 1–Cr–Mo–V and 2.25Cr–1Mo together with the newer higher chrome steels such as 12Cr–1Mo–1 V and 9Cr steels, neither have sufficient rupture strength nor are able to resist oxidation at temperatures much above 923 K. Whilst the nickel-based alloys, such as the Ni–15.5Cr–8Fe alloy, promise much better rupture strength and oxidation resistance at temperatures above 973 K, they are increasingly expensive. Therefore, austenitic steels such as Type 316, Type 316L, Type 304H and Type 347H will be increasingly used in both boiler tubes and perhaps also in pipers and headers in an attempt to raise temperatures. Furthermore, newly developed austenitic stainless steels such as Save 25, Sanicro 25 and BGA4 are likely to be used once creep-rupture data assessments have been performed.

Unfortunately, such creep rupture data assessments of new materials have in the past been both very expensive and protracted requiring the determination of minimum stresses causing rupture in 100,000 h or more. In addition, for several newly developed steels, the allowable strengths have been progressively reduced as measurements from longer-term tests have become available [1–3]. These and other uncertainties have then justified the completion of protracted programmes covering stress–temperature conditions giving creep lives up to 100,000 h or more for multiple batches of many power plant steels [4].

Recently, Wilshire and Battenbough [5] and Wilshire and Scharning [6–9] have developed a new methodology offering the prospect of cost-effective creep-rupture data assessments. Using a variety of low alloy and high chrome steels, these authors have demonstrated that by normalising the applied stress through the appropriate tensile strength, the methodology is capable of accurately predicting, from relatively short-term data, the minimum creep rates, the times to various strains and the creep lives for stress–temperature conditions causing failure in 100,000 h and

M. Evans (✉)
School of Engineering, Swansea University, Singleton Park, Swansea SA2 8PP, UK
e-mail: m.evans@swansea.ac.uk

more. Evans [10] has also recently demonstrated the predictive superiority of this methodology over existing extrapolation procedures using 1Cr–1Mo–0.25V steel as a test-bed material.

If this methodology can be shown to also work well on the existing long-term datasets that are available for Type 316 austenitic stainless steel, then this would provide added confidence in estimating the minimum stresses causing rupture in 100,000 h in austenitic stainless steels from relatively cheaply generated rupture data out to about 5,000 h. This would represent a considerable achievement as most existing parametric procedures, when applied to austenitic steel datasets, tend to be unable to accurately predict longer lives from short-term data at all the available temperatures [11]. For example, in this publication the Soviet Model [12] failed to accurately predict the creep lives for type 316 stainless steel at 773 K. The application of this methodology to Save 25 and BGA5 would then enable these newly developed austenitic stainless steels to be bought into safe operation more cost effective and over a quicker time scale than is currently possible.

This article therefore aims to carry out a comprehensive evaluation of this new methodology when applied to 18Cr–12Ni–1Mo steel (Type 316 stainless steel plate and bars). To achieve this aim this article is structured as follows: In "The data", the NIMS 18Cr–12Ni–1Mo steel dataset is described. In "The Wilshire–Scharning methodology", the Wilshire–Scharning methodology is applied to this dataset. It is shown in this section that the methodology can not accurately predict long-term failure times from short-term data and so the second half of this section modifies the methodology to give a novel approach to life prediction. This modification is shown to be a generalization of the Wilshire–Scharning methodology. "Model Estimation" then presents a simple method for estimating this novel model and "Application to 18Cr–12Ni–Mo steel" applies the model to the dataset described in "The data". In this section, predictions from the new model are also compared to those obtained from the Wilshire–Scharning model and the estimated activation energies for creep are discussed. A concluding section then outlines some proposals for future work.

The data

To evaluate the predictive capabilities of this new methodology this study features 18Cr–12Ni–Mo steel (Type 316 stainless steel bars and plate). For multiple batches of this austenitic product, both the creep and the creep-fracture properties have been documented comprehensively by the National Institute for Materials Science (NIMS), Japan. NIMS creep datasheet Nos. 14B and 15B [13, 14] include information on eight batches of this material (6 bars and 2 plates). Table 1 gives the chemical composition of each of these batches. Bar specimens for the tensile and creep-rupture tests were taken longitudinally from the round bars and each test specimen had a diameter of 10 mm with a gauge length of 50 mm. Plate specimens for the tensile and creep-rupture tests were taken parallel to the rolling direction from the plate and each test specimen had a diameter of 10 mm with a gauge length of 50 mm. Further details on these creep-rupture testing programs can be found in references [13, 14].

These specimens were tested at constant load over a wide range of conditions: 265–20 MPa and 873–1123 K. In addition to minimum creep rate ($\dot{e}_m$) and time to failure (t_F) measurements, listing were also given of the times to attain various strains (t_e) at 0.005, 0.01, 0.02 and 0.05. Also reported were the values of the 0.2% proof stress (τ_Y) and the ultimate tensile strength (τ_{TS}) determined from high-strain ($\sim 10^{-3}$ s^{-1}) tensile tests carried out at the creep temperatures for each batch of steel investigated. Using these freely available NIMS documents, the accuracy with which 100,000 h strengths can be estimated by extrapolation of

Table 1 Composition of 18Cr–12Ni–Mo steel plate and bar

Batch code	Chemical composition (mass percent)													
Requirement:	C ≤0.08	Si ≤1	Mn ≤2	P ≤0.045	S ≤0.03	Ni 10–14	Cr 16–18	Mo 2–3	Cu –	Ti –	Al –	B –	N –	Nb+Ta –
ADA (bar)	0.06	0.46	1.49	0.032	0.026	12.48	17.43	2.49	0.15	0.009	0.025	0.0008	0.0189	0.04
ADB (bar)	0.07	0.73	1.62	0.029	0.019	11.92	16.97	2.45	0.14	0.009	0.022	0.0013	0.0159	0.04
ADC (bar)	0.07	0.81	1.75	0.026	0.010	10.28	16.97	2.44	0.15	0.044	0.04	0.0016	0.0241	0.04
ADD (bar)	0.07	0.58	1.67	0.027	0.011	10.42	17.3	2.37	0.17	0.047	0.03	0.0007	0.0290	0.03
ADE (bar)	0.08	0.67	1.44	0.026	0.009	12.3	17.11	2.31	0.35	0.013	0.006	0.001	0.0186	0.04
ADF (bar)	0.07	0.61	1.41	0.026	0.007	12.18	16.97	2.25	0.34	0.018	0.006	0.0008	0.0218	0.03
AaA (plate)	0.06	0.74	1.70	0.038	0.011	13.04	17.31	2.56	0.30	0.011	0.005	0.0011	0.0192	0.04
AaB (plate)	0.05	0.74	1.74	0.035	0.006	11.19	17.60	2.32	0.28	0.014	0.005	0.0007	0.0230	0.03

short-term results (5,000 h or less) can be assessed against reliable long-term measurements.

The Wilshire–Scharning methodology

The original model

Wilshire and Scharning [6–9] have recently suggested that the applied stress (τ) should be normalized through measured values of ultimate tensile strength (τ_{TS}) so that datasets can be considered over the complete stress range for $\tau/\tau_{TS} = 1$ to $\tau/\tau_{TS} = 0$. Valid relationships devised to quantify creep-rupture measurements must then make it evident not only that $t_F \to 0$ as $\tau/\tau_{TS} \to 1$ but also that $t_F \to \infty$ as $\tau/\tau_{TS} \to 0$. Whilst many formulations of this are possible, Wilshire and Scharning proposed the following:

$$\tau/\tau_{TS} = \exp\left\{-k_1\left[t_F \exp\left(-Q_c^*/RT\right)\right]^{u_1}\right\} \quad (1a)$$

where Q_c^* is the activation energy for lattice self diffusion in the alloy steel matrixes, R is the universal gas constant (8.314 J mol^{-1} K^{-1}) and k_1 and u_1 are parameters that require estimation. Equation 1a is an S-shaped sigmoidal function whose shape over the range one through to zero for differing values of t_F depends on the value for u_1. Equation 1a can be linearized through an appropriate transformation of the normalized stress—in the specification given by Eq. 1a a ln—ln transformation of the normalized stress is required

$$\ln[-\ln(\tau/\tau_{TS})] = \ln(k_1) + u_1 \ln[t_F] - u_1[Q_c^*/RT]. \quad (1b)$$

A plot of $\ln[t_F]$ against $\ln[-\ln(\tau/\tau_{TS})]$ at a single temperature should then produce a straight line with slope $1/u_1$ and variations in temperature should then produce parallel shifts in this line. Alternatively, a plot of $\ln[-\ln(\tau/\tau_{TS})]$ against $\ln[t_F] - [Q_c^*/RT]$ over all temperatures should produce a single straight line with slope u_1. Wilshire and Scharning [6–9] have applied Eq. 1a to a large variety of low alloy and high chrome steels. A typical result obtained from these studies is shown in Fig. 1a for a 1Cr–1Mo–0.25 V steel. Further details on this material and test methods used can be found in references [10, 15].

As can be seen from this figure, the experimental data do not quite behave in the way described by Eq. 1b. The parameters of Eq. 1b appear to differ at stresses above and below a critical value for the normalized stress—a value of around -0.3 for $\ln[-\ln(\tau/\tau_{TS})]$. This 'kinked' behaviour has been observed in all the steels studied so far by Wilshire and Scharning and therefore appears to be a real phenomenon. The fitted kinked line shown in Fig. 1a was estimated from the short-term data only, i.e. from specimens failing at or before 5,000 h. As can be seen, the methodology produces very accurate predictions of the longer-term data.

Wilshire and Scharning have explained this observed kink in terms of creep deformation mechanisms. For example, in their study of Polycrystalline Copper [5] they observed that the kink occurred at the yield stress. This behavioural pattern suggested to them that dislocation processes are dominant at all stress levels, but that strain accumulation within the grains becomes progressively less important as deformation is increasingly confined to the grain boundary zones when the stress is reduced below the yield stress at a given creep temperature.

Figure 1b applies this methodology to the data published by NIMS on Type 316 stainless steel. In this figure the activation energy for self diffusion in the alloy steel matrixes was taken to be the commonly reported value of 280 kJ mol^{-1} [16]. Whilst a well defined kink point is again observable in this dataset at around zero for $\ln[-\ln(\tau/\tau_{TS})]$, a serious problem is also apparent. Above the kink point the longer-term data clearly lie well above the short-term data. So when Eq. 1b—with a kink allowed for—is estimated from short-term data it will obviously fail to accurately predict the longer-term data. This is the first application of this methodology to steel data where this problem has been observed. This suggests that some modification of the Wilshire–Scharning methodology is required for it is to be successfully applied to Type 316 stainless steel.

A proposed modification

Instead of trying to explain the frequently observable kink in terms of where deformation is taking place (within grains or between grains) it is at least conceivable to think that this observed kink is the result of model misspecification. That τ/τ_{TS} and $\ln[t_F \exp(-Q_c^*/RT)]$ follow a sigmoidal relationship (over the range 0–1 for τ/τ_{TS}) makes sound physical and theoretical sense. However, there is no reason to pre-suppose that this sigmoidal relationship has to be given by Eq. 1a. Indeed, a more general family of sigmoidal relationships exists that contains Eq. 1a as a special case. More specifically, consider the following transformation of the normalized stress:

$$\psi[\tau/\tau_{TS}] = \ln\left[\frac{(\tau/\tau_{TS})^{-\lambda} - 1}{\lambda}\right] \quad (2a)$$

Notice that when $\lambda = 1$ this gives the stress transformation $\ln[(1 - \tau/\tau_{TS})/(\tau/\tau_{TS})]$, and when $\lambda = -1$ the transformation is $\ln[1 - \tau/\tau_{TS}]$, but more interestingly as $\lambda \to 0$, the stress transformation tends to $\ln[-\ln(\tau/\tau_{TS})]$—which is of course the one suggested by Wilshire and Scharning. This suggest that a useful generalization of Eq. 1b is

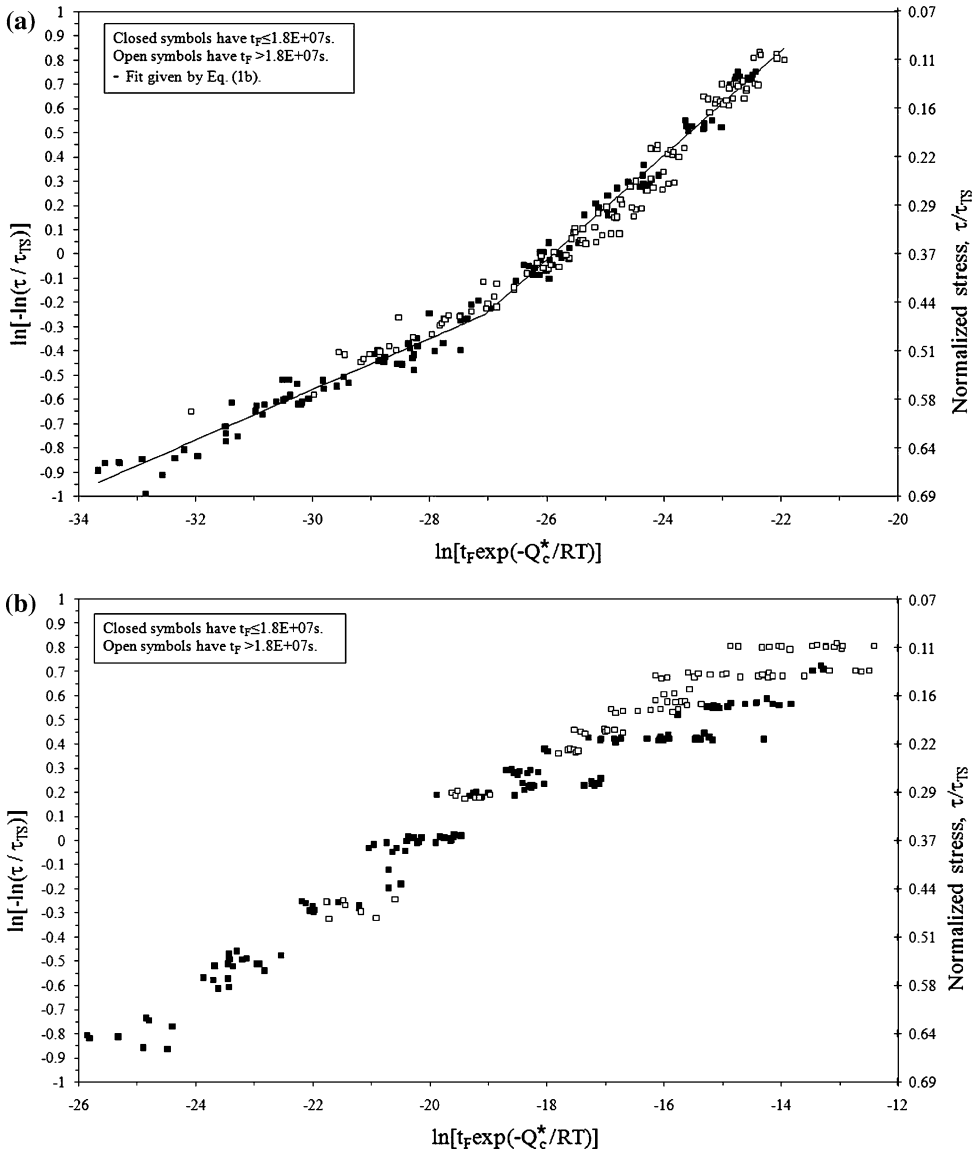

Fig. 1 **a** The dependence of $\ln[t_F \exp(-Q_c^*/RT)]$ on $\ln[-\ln(\tau/\tau_{TS})]$with $Q_c^* = 300\,\mathrm{kJ\,mol^{-1}}$ for 1Cr–1Mo–0.25 V steel at 723–948 K. **b** The dependence of $\ln[t_F \exp(-Q_c^*/RT)]$ on $\ln[-\ln(\tau/\tau_{TS})]$ with $Q_c^* = 300\,\mathrm{kJ\,mol^{-1}}$ for 18Cr–12Ni–Mo steel at 873–1123 K

$$\psi[\tau/\tau_{TS}] = \ln[k_1] + u_1 \ln[t_F] - \omega(T;\Theta) \tag{2b}$$

where $\omega(T;\Theta)$ is some general function of temperature with parameter vector Θ. Expressed in terms of the normalized stress this can be written as

$$\tau/\tau_{TS} = \{1 + \lambda k_1 [t_F \exp(-\omega(T;\Theta))]^{u_1}\}^{-1/\lambda} \tag{2c}$$

If the function $\omega(T;\Theta)$ is linear in $1/T$ (i.e. $\omega(T;\Theta) = Q_c^*/RT$), then as $\lambda \to 0$, Eq. 2c tends to Eq. 1a and so is identical to the Wilshire–Scharning model. When $\lambda = 1$, Eq. 2c simplifies to

$$\ln[(1 - \tau/\tau_{TS})/(\tau/\tau_{TS})] = \ln[k_1] + u_1 \ln[t_F] - \omega(T;\Theta)$$

Equation 2b is more general in the sense that λ can take on values different from zero and it may then be the case that a particular value for λ produces a linear relationship between the transformed normalized stress and $\ln[t_F]$ at a given temperature, i.e. removes the kink in the data. Within this more general framework the kink observed by Wilshire and Scharning can be seen as the result of functional misspecification.

Evidence that Eq. 1b may be a misspecification can be found in some of the low alloy steels studied by Wilshire and Scharning. For example, consider again the NIMS dataset on 1Cr–1Mo–0.25 V steel. In Fig. 2, $\ln[t_F \exp(-Q_c^*/RT)]$ with $Q_c^* = 300\,\mathrm{kJ\,mol^{-1}}$ is plotted against $\psi[\tau/\tau_{TS}]$ when $\lambda = -1$. This corresponds to the stress transformation $\ln[1 - \tau/\tau_{TS}]$ and in comparison with Fig. 1a it is clear that the kink has now all but disappeared.

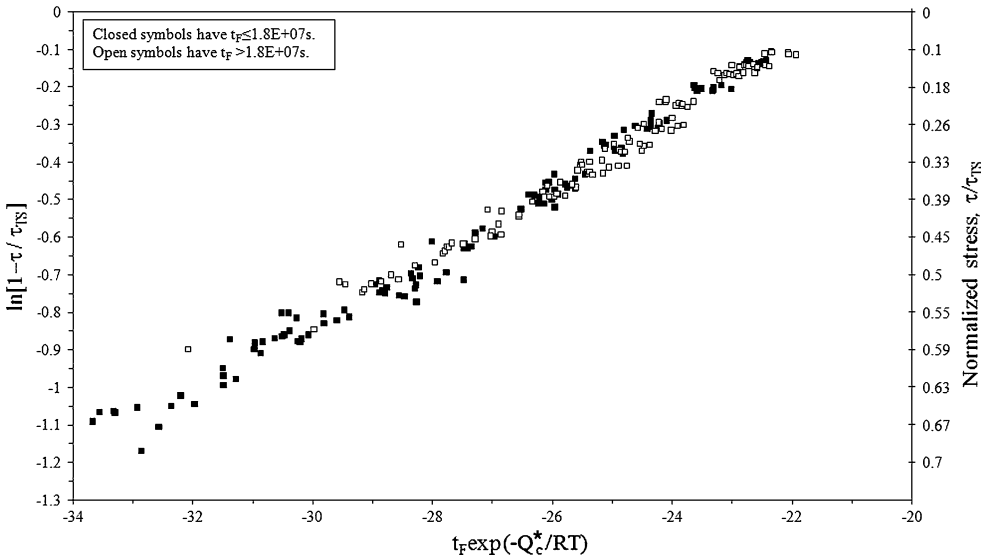

Fig. 2 The dependence of $\ln[t_F \exp(-Q_c^*/RT)]$ on $\ln[1 - \tau/\tau_{TS}]$ with $Q_c^* = 300\,\mathrm{kJ\,mol^{-1}}$ for 1Cr–1Mo–0.25 V steel at 723–948 K

Model estimation

For estimation purposes it is useful to use the following two step procedure. In the first step a baseline function is estimated from short-term failure time data which have been collected at a single temperature—referred to here as the base temperature. This base temperature can be any temperature within the creep database being studied, but ideally should be that temperature at which most specimens are tested. In this article the base temperature chosen from the date set described in "The data" above was taken to be 973 K, $T_{j=B} = 973$ K. At this temperature 63 specimens were tested at a variety of different normalized stresses.

Then working within the ethos of the Wilshire–Scharning methodology, the failure time of a specimen tested at this temperature, $t_F|T_{j=B}$, will also depend upon some transformation, ψ, of the normalized stress at which it is tested. This dependency is given by the following baseline function:

$$\ln[t_F|T_{j=B}] = \delta_0 + \delta_1\{\psi[\tau/\tau_{TS}]\} \tag{3}$$

which is a simple re arrangement of Eq. 2b with $\delta_1 = 1/u_1$ and $\delta_o = -\ln[k_1]/u_1$ with $\omega(T; \Theta) = 0$ as all failure times are at the constant base temperature. When $\lambda = 0$, the transformation of the normalized stress is that proposed by Wilshire and Scharning.

Values for the parameters δ_o, δ_1 and λ are chosen so as to minimize the squared difference between the failure times given by Eq. 3 and the actual failure times over all test specimens that failed at the base temperature within a pre-defined short time span. This difference is called the residual sum of squares (RSS) in the least squares literature. This time span can be any value, but for this article the short term is defined as 5,000 h or less. For a given λ, Eq. 3 is a linear function and so ordinary linear least squares can be used to minimize the residual sum of squares. If this is then repeated for a variety of different λ's, the one that gives the smallest RSS is chosen as the correct value for λ.

In the second step, temperature must be incorporated into the baseline function. To be consistent with the general specification given in "The Wilshire–Scharning methodology" above, this is done in such a way as to ensure that the effect of changing temperature is to either shift the baseline function or more generally to shift and rotate the baseline function. Whether the baseline function shifts or shifts and rotates will depend upon the form of $\omega(T; \Theta)$ in Eq. 4a below:

$$\ln[t_F|T_j] = \delta_0 + \delta_1\{\psi[\tau/\tau_{TS}]\} + \omega(T; \Theta) \tag{4a}$$

where $t_F|T_j$ is the failure time of a specimen tested at any one of the j temperatures making up the database being studied and the δ's are estimated solely from the baseline temperature data. The simplest way to estimate $\omega(T; \Theta)$ is to apply Eq. 4a to each temperature (other than the base temperature) separately. That is, estimate a value for Δ in Eq. 4b below for each temperature

$$\ln[t_F|T_j] = \delta_0 + \delta_1\{\psi[\tau/\tau_{TS}]\} + \Delta_j. \tag{4b}$$

Having estimated the parameters δ_o, δ_1 and λ in Eq. 3, the value for Δ_j at temperature T_j is taken to be that value which minimizes the squared difference between the failure times given by Eq. 4b and the actual failure times over all test specimens that failed at temperature T_j—and within the pre defined short time span. Repeating this procedure for all temperatures will yield a Δ value for each temperature. Then a plot of Δ_j against $1/RT$ (or some other temperature transformation) should help identify the form of $\omega(T; \Theta)$. Take some possibilities. If $\omega(T; \Theta)$ is given by

$$\Delta_j = \omega(T;\Theta) = Q_c^*/RT_j \quad (5a)$$

then variations in temperature shift the baseline function in a parallel fashion—the size of this shift in turn depending on the activation energy for self diffusion. A plot of Δ_j against $1/RT$ will then allow the activation energy to be estimated from the slope of this plot. If

$$\Delta_j = \omega(T;\Theta) = \delta/RT + \delta_3\{\psi[\tau/\tau_{TS}]\}/RT \quad (5b)$$

then variations in temperature shift and rotate the baseline function.

Application to 18Cr–12Ni–Mo steel

Table 2 shows the results of estimating Eq. 3 using least squares when applied to specimens that failed at or before 5,000 h and when tested at 973 K. Two different stress transformations are used—one corresponding to $\lambda = 1$ and one when $\lambda = 0$. In both cases all the estimated parameters (i.e. the δ's) are statistically significant at the 5% level, but the residual sum of squares is smallest when $\lambda = 1$. These results are displayed visually in Fig. 3 where the R^2 value, which gives the percentage variation in log failure times explained by variations in the transformed normalized stress, is highest when $\lambda = 1$. More significant, however, is the fact that when the estimated lines are extrapolated to the longer-term data, the predictions are substantially better when $\lambda = 1$.

Table 2 Values for the parameters of Eq. 3, estimated from specimen on 18Cr–12Ni–Mo steel that failed at or before t_F = 5,000 h at 973 K using linear least squares

Parameter	$\lambda = 1$	$\lambda = 0$
δ_0	12.41* [132.9]	14.45* [296.3]
δ_1	3.64* [29.1]	5.79* [28.5]
RSS	2.48	2.60

* Indicates an estimate that is statistically significant at the 5% level of significance. Student's t values are in *parenthesis*. RSS is the residual sum of squares in Eq. 3. λ has the meaning given by Eq. 2a

Figure 4a shows the estimated values for Δ at each temperature when plotted against $1000/RT$. As can be seen the data seem to support the specification given by Eq. 5a for $\omega(T;\Theta)$. The estimated activation energy for self diffusion is then put at around 193 kJ mol^{-1}—which is substantially lower than what is considered to be the activation energy for self diffusion in this steel matrix—about 280 kJ mol^{-1}. However, this value for Q_c^* can be interpreted as an average activation energy over all temperatures. That is, instead of estimating Q_c^* from the data in Fig. 4a, Δ_j can be seen as the product of the activation energy at temperature T_j and $1000/RT_j$

$$\Delta_j = 1000[Q_c]_j/RT_j$$

so that $[Q_c]_j = \Delta_j RT_j/1000$. Q_c is the activation energy for creep which may be different from the activation energy for self diffusion in the steel matrix. Figure 4b plots these activation energies as calculated from the Δ_j values shown in Fig. 4a. As can be seen the activation energies appear to be highest at the lowest temperatures. This at first sight appears to be a little unusual in that at the higher temperatures bulk diffusion rates should be high so that the measured activation energy should be close to that for self diffusion in the alloy steel matrixes. Yet as can be seen from Fig. 4b, the measured activation energies at the higher temperatures are about half that for self diffusion, Q_c^*.

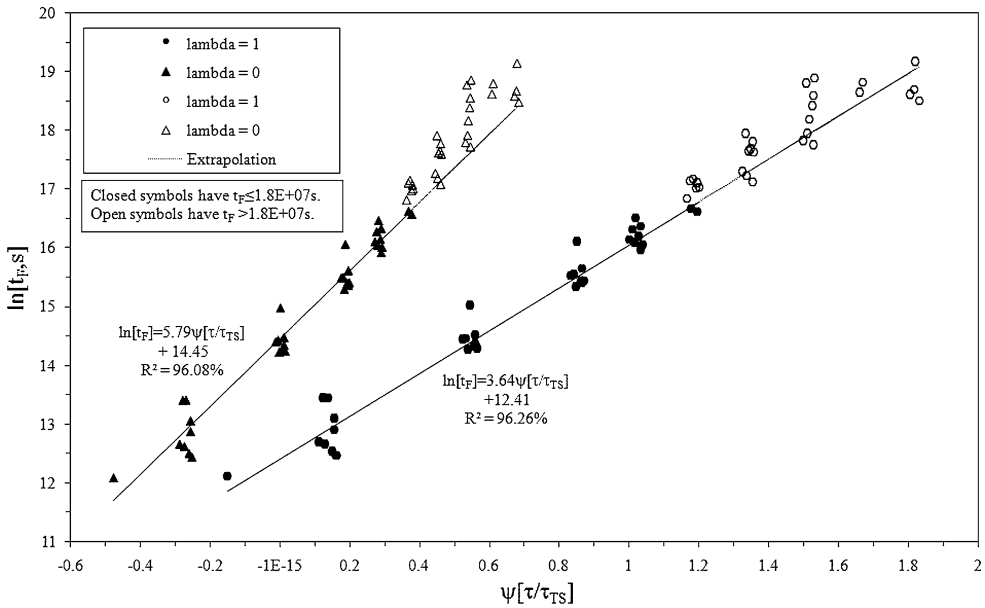

Fig. 3 The dependence of $\ln[t_F]$ on transformations of the normalized stress as defined by Eq. 2a for 18Cr–12Ni–Mo steel at 773 K

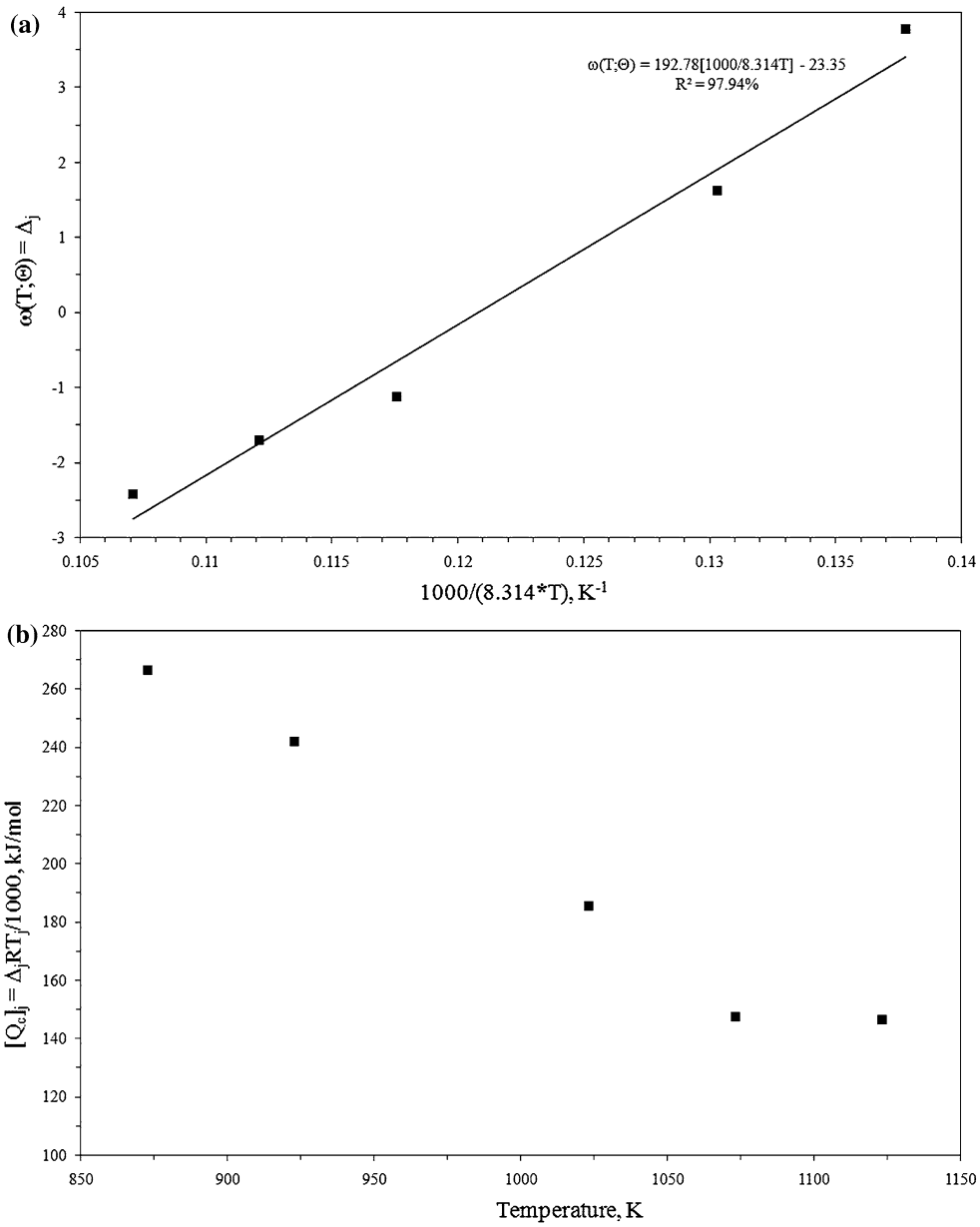

Fig. 4 **a** The dependence of $\omega(T; \Theta)$ on temperature for 18Cr–12Ni–Mo steel. **b** The apparent dependence of activation energies on temperature for 18Cr–12Ni–Mo steel

However, an important characteristic of this NRIM dataset on Type 316 stainless steel is that all the tests carried out at temperatures above 973 K were done at stresses below the yield stress. Then at temperatures below 973 K all the test results were obtained using stresses above the yield stress. This pattern is likely to be important because Wilshire and Willis [17] have recently shown that to account for the observed creep behaviour patterns in this stainless steel at different test conditions and levels of pre straining, it is necessary to recognize the different contributions made by the grain interiors and the grain-boundary zones (comprising grain-boundary sliding and associated deformation in grain regions adjacent to the boundaries) to the overall rates of creep strain accumulation and intergranular damage development. Tertiary acceleration in creep rates are predominantly caused by grain boundary cavitation. This distinction has been described by Gifkins [18] as core and mantle behaviour and in many textbooks on creep in steels, as bulk and grain boundary/dislocation core diffusion (see for example Ashby and Jones [19]).

The above results are then explained in terms of the contributions made by the grain interiors and the grain-boundary zones to the overall creep rate, with the minimum creep rate decreasing rapidly towards zero when deformation in increasingly confined to the boundary zones as the stress decreases below the yield stress. This is important because grain boundaries provide rapid diffusion paths characterized by activation energies lower than that for self diffusion in the alloy steel matrixes. In such a situation the measured activation energy will no longer be that for self

diffusion in the alloy steel matrixes, but a lower value associated with these easier paths.

Thus, Fig. 4b is not really showing the effect of temperature on the measured activation energy, but the fact that the stress falls below the yield stress at the higher temperatures. Figure 4b therefore suggests that the activation energy for self diffusion (through the crystal lattice) is around 250 kJ mol^{-1}, whilst the activation energy for pipe diffusion (self diffusion at grain boundaries or dislocation cores) is around 170 kJ mol^{-1}.

Having interpreted the estimate made of $\omega(T;\Theta)$ from the short-term data, the final step is to use this function, in conjunction with the baseline function, to predict the longer-term failure times. The full model used to do this is

$$\ln[t_F|T_j] = 12.41 + 3.64\ln\{(1-\tau/\tau_{TS})/(\tau/\tau_{TS})\} + 193T^* \quad (6a)$$

where $T^* = 1000/(8.314T) - 1000/(8.314[973])$. This temperature transformation is used so that $\omega(T;\Theta) = 0$ at the base temperature. The results of this are shown in Fig. 5a. Note that the effect of temperature is to shift the baseline function in a parallel fashion and this appears to result in accurate life time predictions at each temperature—even out to the longest failure times. The exception to this conclusion being those tests carried out at 873 K. At this relatively low temperature the specification of $\omega(T;\Theta)$ appears to be inadequate and an inspection of Fig. 5a suggests that the slope at this temperature should be steeper than that at all the others. This can be dealt with by Eq. 5b. Figure 5b shows the predictions obtained using the model

$$\begin{aligned}\ln[t_F|T_j] =& 12.41 + 3.64\ln\{(1-\tau\tau_{TS})/(\tau\tau_{TS})\} + 201T^* \\ &+ 62\ln\{(1-\tau\tau_{TS})/(\tau\tau_{TS})\}T^* \\ &\text{when } T = 873\,\text{K} \\ \ln[t_F|T_j] =& 12.41 + 3.64\ln\{1-[\tau\tau_{TS}]\} + 201T^* \quad \text{otherwise}\end{aligned} \quad (6b)$$

It can be seen from this figure that the prediction for times to failure at 873 K are now dramatically improved. As a comparative exercise it is interesting to compare these predictions with those that would have been obtained through the normal application of the Wilshire–Scharning methodology. This is essentially Eq. 3 with $\lambda = 0$ and $\omega(T;\Theta) = 192T^*$. This is shown in Fig. 5c. In comparison to Fig. 5b it can be seen that the predictions are much worse. For example, at 973 K, the Wilshire–Scharning predictions are right at the lower end of the recorded failure times.

Finally, Fig. 6 shows the predictions in Fig. 5b within the more familiar setting where predicted failure times are plotted against stress—rather than the normalized stress. To do this, the average tensile strength at each temperature was used to obtain the prediction curves shown in Fig. 6. The model appears to be capable of accurately predicting lives out to 100,000 h from data recorded up to only 5,000 h.

Conclusions

This article has demonstrated that the Wilshire–Scharning methodology, in its original format, is not capable of producing (using only short-term data) accurate long-term predictions of the lives of 18Cr–12Ni–Mo steel. A modification of the Wilshire–Scharning methodology was put forward in this article that had the potential to increase the predictive accuracy of this methodology when applied to this material. This modification is a generalization of the Wilshire–Scharning methodology in that it contains this original model as a special case.

When this modified methodology was applied to 18Cr–12Ni–Mo steel, it was found that the best predictions of longer-term times to failure were obtained when the normalized stress was transformed to $\ln[(1-\tau/\tau_{TS})/(\tau/\tau_{TS})]$—rather than the more familiar $\ln[-\ln(\tau/\tau_{TS})]$ transformation. Plots of $\ln[t_F]$ against this transformation produced straight lines at constant temperature and so removed the need to model "kinks" in the relationship. It was also found that the measured activation energy was dependent upon the yield stress with an activation energy for creep of around 250 kJ mol^{-1} above the yield stress and about half the quantity below the yield stress. This could be attributable to the domination of pipe diffusion at very low stresses [17]. This modified methodology produced very accurate predictions of the failure time values reported for stress–temperature combinations giving creep lives of 100,000 h or more.

It is hoped that this modified methodology will be general enough to allow accurate predictions to be made of the safe life of new and developing high temperature materials from relatively short-term datasets. If so, this will enable these newly developed austenitic stainless steels to be bought into safe operation more cost effectively and over a quicker time scale than is currently possible. This in turn will bring considerable economic benefits to power generating companies who will then have the capability to safely increase the operating temperatures of their plants. One area for future work, therefore, includes further verification of this modified methodology on currently available high-strength austenitic steels such as Esshete 1250, AC66, Type 316L(N) and Type 316LNB stainless steels (for which extensive long-term datasets are available) as well as on newly developed high-strength austenitic steels such as Save 25 and Sanicro 25 (where large datasets are not so readily available). Another area would be to

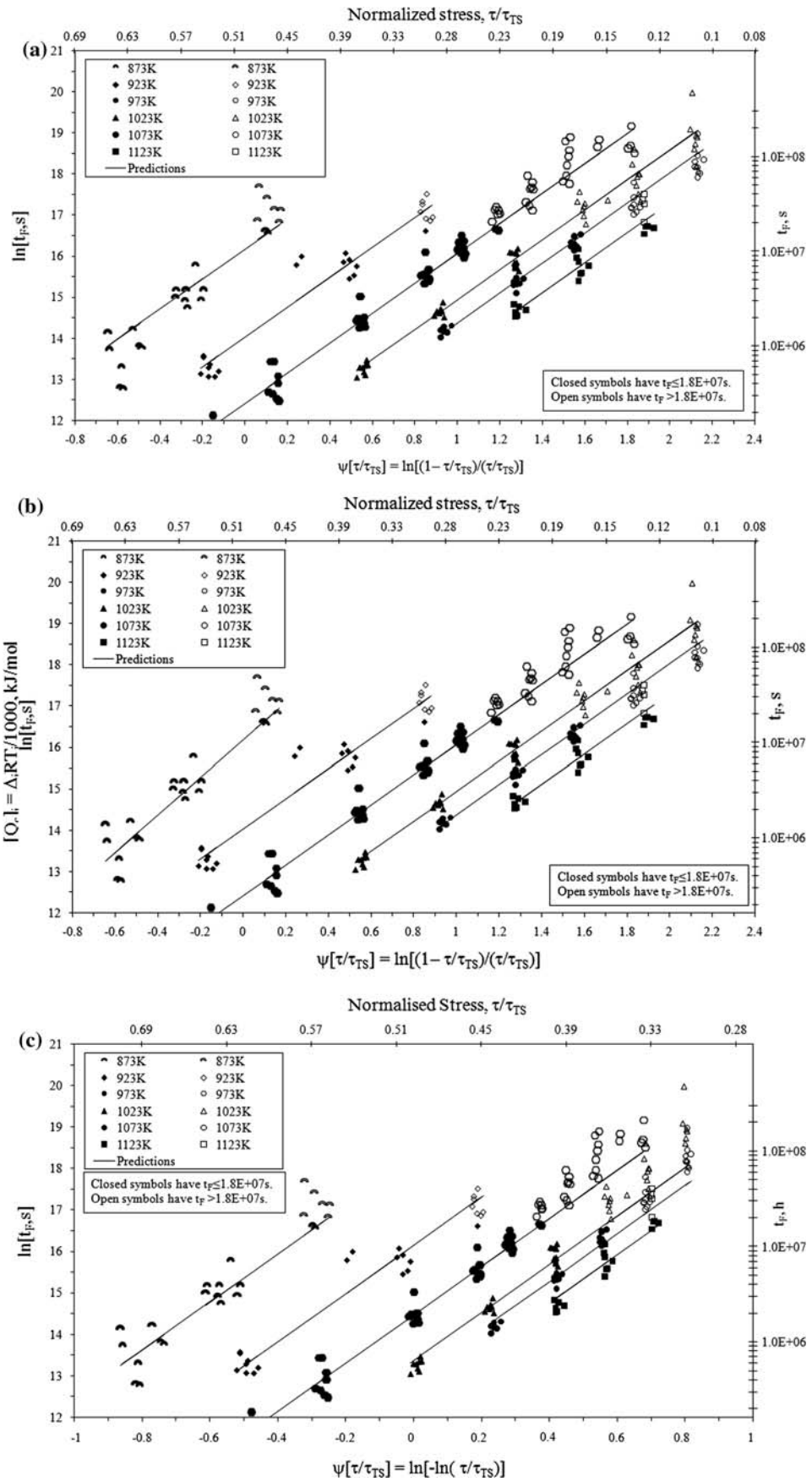

Fig. 5 Predicted lifetimes for 18Cr–12Ni–Mo steel at 873–1123 K using **a** Eq. 6a, **b** Eq. 6b, **c** the Wilshire–Sharning methodology

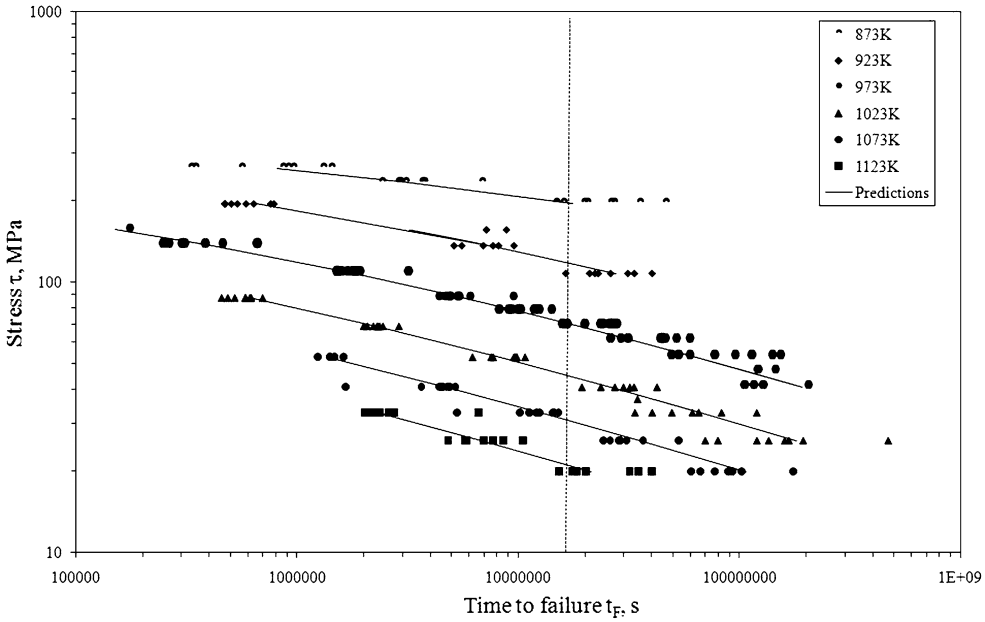

Fig. 6 Predicted lifetimes as a function of stress for 18Cr–12Ni–Mo steel at 873–1123 K using Eq. 6b

incorporate the multilevel structure (involving the casts selected for testing and the individual specimens tested for each cast) of creep databases into the methodology developed in this article.

References

1. Bendrick W, Gabrel J (2005) In: Shibli IA et al (eds) Creep and fracture in high temperature components—design and life assessment issues. DEStech Publ. Inc, London, p 406
2. Kimura K (2005) In: Shibli IA et al (eds) Creep and fracture in high temperature components—design and life assessment issues. DEStech Publ. Inc, London, p 1009
3. Cipolla L, Gabrel J (2005) In: Super-high strength steels. Associazione Italia di metallurgia, Rome, CD ROM
4. Yagi K (2005) In: Shibli IA et al (eds) Creep and fracture in high temperature components—design and life assessment issues. DEStech Publ. Inc, London, p 31
5. Wilshire B, Battenbough AJ (2007) Mater Sci Eng A 443:156
6. Wilshire B, Scharning PJ (2008) Mater Sci Technol 24:1
7. Wilshire B, Scharning PJ (2008) Int Mater Rev 53:91
8. Wilshire B, Scharning PJ (2009) Mater Sci Technol 25:242
9. Wilshire B, Scharning PJ, Hurst R (2009) Mater Sci Eng A 510–511:3
10. Evans M (2009) J Eng Mater Technol 131:021011
11. Spindler MW, Andersson H (2007) In: Viswanathan R, Gandy D, Coleman K (eds) Advances in materials technology for fossil power plants, proceedings from the fifth international conference, Marco Island, FL, October 3–5, 2007, pp 702–717
12. Trunin II, Golobova NG, Loginov EA (1971) In: Proceedings of the 4th international symposium on heat resistant metallic materials. Mala Fatra: CSSR, p 168
13. NIMS Creep Data Sheet No. 14B (1988)
14. NIMS Creep Data Sheet No. 15B (1988)
15. NIMS Creep Data Sheet No. 9B (1990)
16. Rieth M (2007) J Nuclear Mater 367:915
17. Wilshire B, Willis M (2004) Metall Mater Trans A 35A:563
18. Gifkins RC (1976) Metall Trans 7A:1225
19. Ashby MF, Jones DRH (1996) Engineering materials 1: an introduction to their properties and applications, Chap. 19. Butterworth-Heinemann, Oxford